NUCL SCI TECH (2016) 27:58
DOI 10.1007/s41365-016-0062-1

An inversion decomposition method for better energy resolution of NaI(Tl) scintillation detectors based on a Gaussian response matrix

Jian-Feng He[1,2] · Yao-Zong Yang[3] · Jin-Hui Qu[1] · Qi-Fan Wu[2] · Hai-Ling Xiao[1] · Cong-Cong Yu[4]

Received: 10 December 2014 / Revised: 14 March 2016 / Accepted: 24 March 2016 / Published online: 9 May 2016

Abstract NaI(Tl) scintillation detectors have been widely applied for gamma-ray spectrum measurements owing to advantages such as high detection efficiency and low price. However, the mitigation of the limited energy resolution of these detectors, which detracts from an accurate analysis of the instrument spectra obtained, remains a crucial need. Based on the physical properties and spectrum formation processes of NaI(Tl) scintillation detectors, the detector response to gamma photons with different energies is represented by photopeaks that are approximately Gaussian in shape with unique full-width-at-half-maximum (FWHM) values. The FWHM is established as a detector parameter based on resolution calibrations and is used in the construction of a general Gaussian response matrix, which is employed for the inverse decomposition of gamma spectra obtained from the detector. The Gold and Boosted Gold iterative algorithms are employed to accelerate the decomposition of the measured spectrum. Tests of the inverse decomposition method on multiple simulated overlapping peaks and on experimentally obtained U and Th radionuclide series spectra verify the practicability of the method, particularly in the low-energy region of the spectrum, providing for the accurate qualitative and quantitative analysis of radionuclides.

Keywords NaI(Tl) scintillation detector · Gamma-ray energy spectrum · Gaussian response matrix · Inversion decomposition

1 Introduction

Resolving the complex gamma-ray energy spectrum data obtained in gamma spectrometry is a key process in nuclear analysis, and the accuracy of this process is greatly affected by the choice of detector. NaI(Tl) scintillation detectors have been widely employed in gamma spectrometry systems owing to advantages such as high detection efficiency and low price [1, 2]. However, the limited energy resolution of NaI(Tl) scintillation detectors results in the overlapping of photopeaks of similar energy, making them difficult to distinguish. Moreover, the Compton scattering generated by gamma photons in the NaI(Tl) crystal results in the superposition of spectrum lines with a large number of low-energy components, which increases the number of gamma rays in the low-energy range, resulting in fuzzy peak boundaries, particularly in a high background environment. As such, the rate of correct radionuclide identification is decreased. The

This work was supported by the National Natural Science Foundation of China (Grant No. 11365001), National Major Scientific Equipment Development Projects (Grant No. 041514065), the Educational Commission of Jiangxi Province of China (Grant No. GJJ13464), Plan of Science and Technology of Jiangxi Province (Grant No. 20141BBE50024), and the Fundamental Science on Radioactive Geology and Exploration Technology Laboratory, East China Institute of Technology (Grant No. RGET1316).

✉ Jian-Feng He
hjf_10@yeah.net

[1] Fundamental Science on Radioactive Geology and Exploration Technology Laboratory, East China Institute of Technology, Nanchang 330013, China

[2] Department of Engineering Physics, Tsinghua University, Beijing 100084, China

[3] Jiujiang Power Supply Subsidiary Company of State Grid Jianxi Electronic Power Company, Jiujiang 332000, China

[4] Sichuan Integrative Medicine Hospital Sub-health Testing and Evaluation Laboratory, Chengdu 610041, China

problem is further compounded for spectra comprised of numerous types of nuclides, wherein the processing algorithm required for decomposing such spectra must itself be of significantly greater complexity. An analysis of conventional gamma energy spectrum processing mainly includes spectrum line smoothing, peak search, determination of peak borders, background subtraction, overlapping peak decomposition, net area peak calculation and activity, and a series of forward modeling processes and methods [3–5]. However, the qualitative and quantitative analytical results obtained by conventional methods generally deviate quite significantly from their actual values [6]. Therefore, this study seeks to apply an inversion analysis method for the energy spectrum data obtained from NaI(Tl) scintillation detectors.

At the same time, compared with the author's article to be published and named "An inversion decomposition test based on Monte Carlo response matrix on the gamma-ray spectra from NaI(Tl) scintillation detector" [7], there are many different novelties. First of all, the different constructed methods of response matrix: The Monte Carlo response matrix is established by the Monte Carlo method to simulate γ photons with the NaI(Tl) scintillation detector interaction. And the Gaussian response matrix is constructed by the response to gamma photons of different energies in the NaI(T1) detector which corresponds to approximately Gaussian photoelectric peaks with unique FWHM values, and the FWHM is established as a detector parameter based on resolution calibrations. Secondly, the different decomposition processes of spectral: The Monte Carlo response matrix to decompose γ-spectra in practical applications is subject to certain restrictions, such as the scintillation detector sizes, the detector energy resolution, the scattering background, the distance between the source and the detector, and distance between the source and the sample, but it eliminates the need for spectral peak searching, background subtraction, overlapping peaks decomposition and is widely used in the study. The decomposition of the measured spectra with Gaussian response matrix needs to smooth spectra, peak search and boundary determination, background subtraction and other processes, which it makes spectral analytical accuracy affected to some degree. But the Gaussian response matrix has a small capacity of computation, and if choosing the calibration model of the FWHM, it can be subtracted from the background of the full spectral. It should be related to the detectors, unrelated to the measurement conditions and environment, thus it can have practical applications. So, the proposed method is based on building a Gaussian response matrix mediating between an actual gamma radiation source spectrum and an experimentally obtained spectrum, that, in combination with the Gold and Boosted Gold algorithms, achieves rapid and accurate decomposition of the highly convoluted photopeaks obtained from low-resolution NaI(Tl) scintillation detectors.

2 Principle of deconvolution and construction of the Gaussian response matrix

The gamma spectral characteristics obtained from gamma spectrometry systems reflect the interaction between gamma rays and materials. On the one hand, the characteristics of spectral data are related to nuclide decay, whereas, on the other hand, it is closely related to the performance of the detector. Because the luminous efficiency is not absolutely uniform in an NaI(Tl) scintillation, the number of photons collected is related to the location of the scintillation event, the resulting number of photoelectrons will also vary, and the multiplier of the photomultiplier tubes will exhibit fluctuation as well. Therefore, the output pulse amplitude created by the scintillation detector exhibits a slight fluctuation about a mean value. The detector characteristics corresponding to the response of the NaI(T1) crystal and the physical properties of the spectrum formation process result in a peak shape that can be well approximated by a Gaussian function [8, 9]. Therefore, the gamma spectrum of a single-energy peak response obtained by a scintillation detector is assumed to approximately obey the following Gaussian distribution [8, 9].

$$f(x) = \frac{1}{\sqrt{2\pi}\sigma} e^{-(x-\mu)^2/2\sigma^2} \tag{1}$$

Here, σ is a parameter reflecting the peak distribution width (variance), and μ is the energy channel number at the center of the peak. The full width at half maximum (FWHM) of a Gaussian peak is related to σ according to the expression $\mathrm{FWHM} = 2\sqrt{2\ln 2}\sigma = 2.355\sigma$. Due to the characteristics of the scintillation detector and the physical properties of spectrum formation, the response to gamma photons of different energies in the NaI(T1) detector corresponds to approximately Gaussian photoelectric peaks with unique FWHM values.

2.1 Gaussian deconvolution method

With the continuing development of signal and system theory in conjunction with developing computer technology, convolution methods have been widely applied, and increasing attention has also been devoted to deconvolution methods [10–12]. Deconvolution is the inverse operation of convolution. Gaussian deconvolution involves inverse convolution based on a response matrix represented by a Gaussian function matrix. Convolution can be employed to solve the zero-state response of a system to an arbitrary excitation signal using the impulse response $r(t)$ of the system in the time domain [13, 14]. The convolution formula is as follows:

$$y(t) = x(t) * r(t), \tag{2}$$

where $r(t)$ is the measured response spectrum, $x(t)$ is the input spectrum, and the symbol "*" represents convolution. After variable substitution, convolution can be given in integral form as

$$y(t) = \int_{-\infty}^{\infty} x(\tau) r(t-\tau) \mathrm{d}\tau. \tag{3}$$

For discrete data, convolution is given as

$$y(n) = \sum_{m=-\infty}^{\infty} x(m) r(n-m), \tag{4}$$

where $y(n)$ is the measured response spectrum in n channels, $x(m)$ is the input spectrum in m channels, and, for a discrete finite sequence comprised of an input sequence of N components and a response sequence of M components, is given as

$$y(n) = \sum_{m=0}^{N-1} x(m) r(n-m), \quad n = 0, 1, 2 \ldots N + M - 1. \tag{5}$$

Equation (5) can be written in matrix form as follows:

$$\begin{bmatrix} y(0) \\ y(1) \\ \vdots \\ y(N+M-2) \\ y(N+M-1) \end{bmatrix} = \begin{bmatrix} r(0) & 0 & 0 & 0 & \cdots & 0 \\ r(1) & r(0) & 0 & 0 & \cdots & 0 \\ \vdots & r(1) & r(0) & 0 & \cdots & 0 \\ r(M-1) & \vdots & r(1) & r(0) & \cdots & 0 \\ 0 & r(M-1) & \vdots & r(1) & r(0) & 0 \\ 0 & 0 & r(M-1) & \vdots & r(1) & r(0) \\ 0 & 0 & 0 & r(M-1) & \ddots & r(1) \\ \vdots & \vdots & \vdots & \vdots & \ddots & \vdots \\ 0 & 0 & 0 & 0 & \cdots & r(M-1) \end{bmatrix} \begin{bmatrix} x(0) \\ x(1) \\ x(2) \\ \vdots \\ \vdots \\ x(N-1) \end{bmatrix}, \tag{6}$$

here, the $r(\cdot)$ values are the normalized counts of system response and represent the Gaussian peak shapes employed in Gaussian deconvolution. For simplicity, Eq. (6) is written as

$$\boldsymbol{y} = R \cdot \boldsymbol{x}. \tag{7}$$

Based upon the expression given in Eq. (7), deconvolution involves obtaining the actual system input $\boldsymbol{x}$ based upon a known output $\boldsymbol{y}$ of a detection system and an assumed system response R.

2.2 Resolution calibration

The Gaussian peak function fitting method employs initial calibration measurements to calculate the FWHM and the energy resolution of photopeaks measured from single gamma-ray sources [15, 16]. The square of the resolution δ and gamma-ray energy E satisfy the following linear relationship:

$$\delta^2 = a + (b/E), \tag{8}$$

where a and b are fitting constants. Therefore, the calibration values of δ^2 are plotted as the ordinate and the values of $1/E$ as the abscissa, and a and b are obtained from a least-squares fitting of the resulting straight line. The value of δ^2 can be determined for any gamma-ray energy according to Eq. (8).

To this end, gamma spectra derived from ^{241}Am (59.5 keV), ^{57}Co (122.06 and 136.47 keV), ^{134}Cs (795.8 keV), ^{137}Cs (662 keV), ^{60}Co (1173 and 1332 keV), ^{214}Bi (^{238}U series: 1764 keV), and ^{208}Tl (^{232}Th series: 2614 keV) sources were, respectively, collected by an NaI(Tl) scintillation detector using an MCA8000A multichannel pulse amplitude analyzer and supporting software. The characteristic peaks were then extracted, and the FWHM of each characteristic peak was calculated. The FWHM is obtained according to the following calibration formula:

$$\delta = \frac{\mathrm{FWHM}}{E} = \sqrt{a + (b/E)}. \tag{9}$$

To convert a nonlinear least-square fitting into a linear least-square fitting, Eq. (9) is written as a quadratic polynomial:

$$(\mathrm{FWHM})^2 = a \times E^2 + b \times E + c, \tag{10}$$

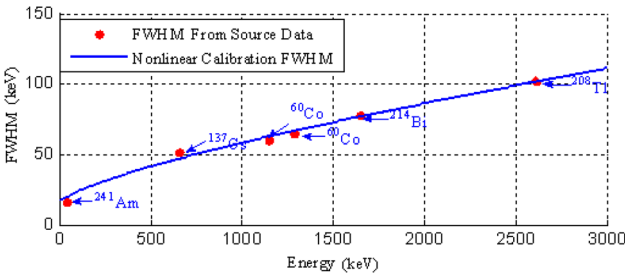

Fig. 1 Nonlinear calibration of the FWHM

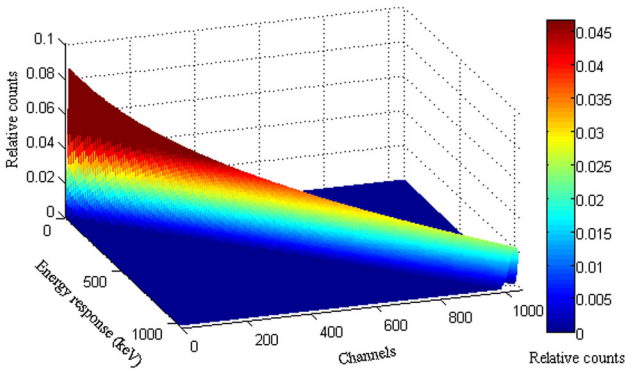

Fig. 3 Adaptive FWHM generated Gaussian function response matrix in three dimensions

where c is constant. The FWHM calibration curve obtained is shown in Fig. 1.

2.3 Construction of the Gaussian response matrix

An impulse response in the form of a Gaussian peak is employed to obtain the corresponding input spectrum through deconvolution. Because the FWHM of spectrum lines varies nonlinearly with respect to the mean photon energy, calculating the impulse response with a single Gaussian function is not appropriate. Therefore, the Gaussian response matrix is formed according to the FWHM to analyze gamma spectrometry data accurately. In addition, a normalized Gaussian response matrix was employed to ensure that the peak area was not altered. The Gaussian function response matrix generated according to the different FWHM values obtained from the nonlinear FWHM calibration given in Eq. (10), i.e., adaptive FWHM, is shown in Fig. 2. The Gaussian response matrix generated by adaptive FWHM in three-dimensional coordinates is shown in Fig. 3.

Figure 2 shows that changes in the peak height and FWHM accord with the response trend of the detector. In addition, as shown in Figs. 2 or 3, there is a phenomenon that Gaussian peak in the energy spectrum section appears "truncate," which is due to the limited Gaussian peaks sample that was truncated. The Gaussian function is an approximation of the peak shape of the detector's response; however, the Gaussian peak is composed of an infinite number of points, and it is impossible to take the infinite number of points when decomposing spectra. So, it needs to determine an appropriate number of points (or length) approaching the peak widths (2 × FWHM), slightly wider than the peak widths or slightly narrower than the peak widths. In practical applications, it has been shown that taking a number of points given by 2 × FWHM ± 1/3/5 is viable, whereas taking more points is slightly better. 1/3/5 can be obtained based on the valuation of Gaussian peak confidence intervals. Here, the number of points is 2 × FWHM + 3. A three-dimensional plot of the Gaussian response matrix is shown in Fig. 3. As shown in Fig. 3, the overall response matrix can be characterized by a spectral peak that presents and changes uniformly with respect to energy, which is the result of the FWHM being rounded. The overall response matrix accords with the actual trends of the FWHM.

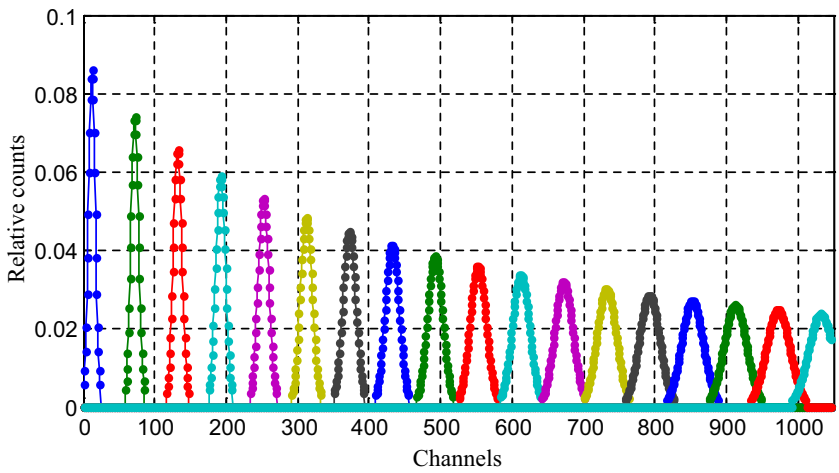

Fig. 2 Adaptive FWHM generated Gaussian function response matrix

3 Solution algorithm

Another problem for analyzing a continuous spectrum is the stability of the response matrix. The results of deconvolution involving Eq. (7) are highly affected by noise, although noise is inescapable during nuclear radiation measurements. As such, deconvolution results may not be accurate, or even unattainable. From the perspective of numerical analysis, the response matrix represents an ill-posed problem associated with solving systems of linear equations within the scope of experimental error. Therefore, the nonlinear iterative Gold and Boosted Gold algorithms, which have shown excellent stability, are used to approach the stable point. The basic characteristic of these algorithms is that the solution is always positive, which is a very important characteristic with respect to gamma energy spectral data [17, 18].

3.1 Gold decomposition algorithm

Gold algorithms have been presented in detail in numerous reports [16–20]. The standard algorithm is based on the van Cittert decomposition algorithm [19–22]. Equation (7) is multiplied by R^T on both sides to obtain a Toeplitz linear system of equations:

$$A \cdot x = b, \tag{11}$$

where $A = R^T R$ and $b = R^T y$. Equation (11) is restructured to facilitate an iterative method of solution. The results in the $(k + 1)$ step can be represented as

$$x^{(k+1)} = x^{(k)} + \xi(b - A \cdot x). \tag{12}$$

Here, a vector sequence $x^{(0)}$ can be obtained for any initial vector $\{x^{(k)}\}_0^{\infty}$. During the iterative solution of a Toeplitz linear system of equations, the value of $\mathbf{x}^{(k+1)}$ is defined as the original value $\mathbf{x}^{(k)}$ plus a variable quantity multiplied a relaxation factor ξ. ξ is employed by introducing the local variable relaxation factor ξ_i:

$$x_i^{(k+1)} = x_i^{(k)} + \frac{x_i^{(k)}}{\sum_{m=1}^{N} A_{im} x_m^{(k)}} \left[b_i - \sum_{m=1}^{N} A_{im} x_m^{(k)} \right]. \tag{13}$$

ξ_i is substituted into Eq. (12) to obtain

$$x_i^{(k+1)} = x_i^{(k)} + \frac{x_i^{(k)}}{\sum_{m=1}^{N} A_{im} x_m^{(k)}} \left[b_i - \sum_{m=1}^{N} A_{im} x_m^{(k)} \right]. \tag{14}$$

Expansion of Eq. (14) yields

$$x_i^{(k+1)} = \frac{b_i}{\sum_{m=1}^{N} A_{im} x_m^{(k)}} x_i^{(k)}, \quad i \in \{0, 1, \ldots, N-1\},\ k \in \{0, 1, \ldots, L\}. \tag{15}$$

The iteration algorithm begins with an initial solution, which is assumed to be

$$x^{(0)} = [1, 1, \ldots, 1]^T. \tag{16}$$

Equation (15) is the Gold algorithm of deconvolution, where L is the iteration number. It can be shown that, if $A_{im} \geq 0$ and $x_i^{(k+1)}$, $i \in \{0, 1, \ldots, N-1\}$, then $x_i^{(k+1)}$, $k \in \{0, 1, \ldots, L\}$ are also always positive, which is quite suitable for spectral data that are, themselves, always positive.

3.2 The improved boosted gold decomposition algorithm

The Gold algorithm was found to quickly converge to a stable value. While continuing to shrink the width of the spectrum peak, it was found that the solution process required halting once the solution reached a steady-state value of $x^{(L)}$, and then, the process was repeated with a new value of $\mathbf{x}^{(0)}$ based on a somewhat altered version of $x^{(L)}$. In response, the power function (i.e., $y = x^a (a > 0, x > 0)$, function is a monotonically increasing) was employed to alter the particular solution, which was found to provide good results. The analytical algorithm of this improved approach is discussed as follows [23]. First of all, set $x^{(0)} = 1$, the value of L, the number of iterations S for which the process is to be repeated, and the process number index $s = 1$. Obtain $r \neq R$ using Eq. (15). Afterward, set $s = s + 1$ and repeat until $s = S$, where the initial input values for subsequent iterations are $x_i^{(0)} = \left| x_i^{(L)} \right|^p$, $i = 0, 1, \ldots, N-1$. Here, an accelerating enhancement operation is conducted based on an acceleration index p.

4 Test and analysis of the inversion decomposition of gamma spectra

In the analytic process, operations providing for peak smoothness, peak search, and nuclide identification are required for qualitative analysis, whereas the determination of peak borders, background subtraction, decomposition of overlapping peaks, and the determination of peak area are required for quantitative analysis. The proposed deconvolution method based on inverse analysis using the constructed Gaussian response matrix was applied to analyze the ^{238}U series and ^{232}Th series spectra lines obtained with an NaI(Tl) scintillation detector. The test analysis results were evaluated for determining the feasibility of the proposed method in practical applications.

4.1 Decomposition of multiple synthesized spectra

For the artificial radionuclide ^{137}Cs (spectral peak energy: 661.6 keV) and natural radionuclides ^{214}Bi (^{238}U series, spectral peak energy: 609 keV) and ^{208}Tl (^{232}Th series, spectral peak energy: 583 keV), the low-resolution NaI(Tl) detector provides overlapping peaks. The Monte Carlo N-particle (MCNP) transport code was applied to simulate an NaI(Tl) detector with a resolution of about 8 % and spectrum lines generated by ^{214}Bi, ^{137}Cs, and ^{208}Tl radionuclides in different proportions. Three simulated samples were created, where Sample 1 employed ^{214}Bi:^{137}Cs:^{208}Tl ratios of 1:1:1, Sample 2 ^{214}Bi:^{137}Cs:^{208}Tl ratios of 2:1:2, and Sample 3 ^{214}Bi:^{137}Cs:^{208}Tl ratios of 2:1:3. Thereby, the performance of the Gaussian deconvolution response matrix for decomposing overlapping peaks could be evaluated directly according to deviations in the relative peak areas of the various samples obtained from deconvolution from those of the actual values.

The results of the Gaussian response matrix deconvolution for the three samples are listed in Table 1. Aside from the deviation for ^{208}Tl of 2.1 % obtained for Sample 3, the deviations of the remaining radionuclides were all less than 1.5 %. Maximum deviations within the allowable range do not affect the accuracy of the qualitative and quantitative analyses of nuclides. The peak area calculated by this method was greatly affected by background subtraction.

Figures 4, 5, and 6 present the respective results of deconvolution for the three samples. The synthetic spectra were obtained by linear superposition of the other three simulated spectra. It is to prove that Gaussian response matrix with adaptive FWHM to decompose spectra with overlapping peak is feasible. From the obtained peak positions given by the channel values within the arrows, it is seen that the deviations between the actual peak positions and those obtained from deconvolution were not greater than one channel. As such, the extent of the deviation was directly related to the total number of channels. Because the number of channels must be an integer, peak positions located near the middle of two channels were easily affected by statistical fluctuations, and the channel address deviated to the left or right of the actual peak position. For example, the peak energy of ^{137}Cs was 661.6 keV, and the spectral energy calibration was

Table 1 Results of the inversion decomposition of overlapping peaks based on the Gaussian response matrix

Sample				Results		Peak area ratio deviation (%)
Number	Nuclide	Peak area	Peak area ratio	Peak area of inversion decomposition	Peak area ratio	
1	^{214}Bi	3.485	0.340	3.280	0.325	−1.5
	^{137}Cs	3.131	0.305	3.166	0.314	0.9
	^{208}Tl	3.644	0.355	3.644	0.361	0.6
2	^{214}Bi	6.970	0.401	7.130	0.414	1.3
	^{137}Cs	3.131	0.180	3.031	0.176	−0.4
	^{208}Tl	7.288	0.419	7.072	0.410	−0.9
3	^{214}Bi	10.455	0.501	10.698	0.516	1.5
	^{137}Cs	3.131	0.150	3.244	0.156	0.6
	^{208}Tl	7.288	0.349	6.793	0.328	−2.1

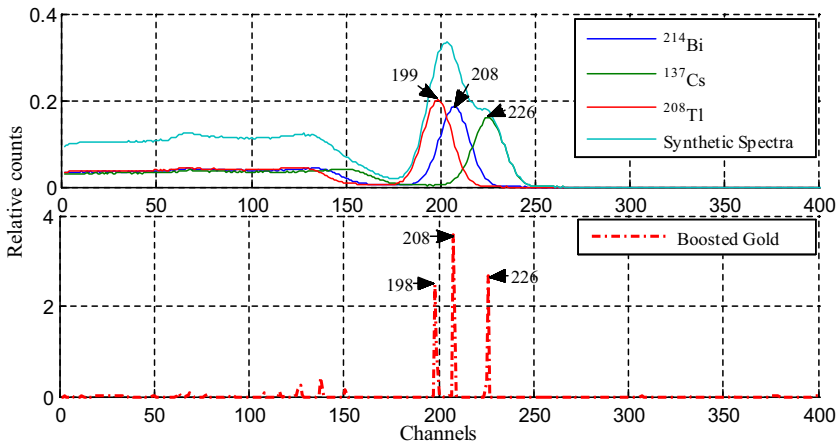

Fig. 4 Sample 1 results of Gaussian response matrix inversion decomposition

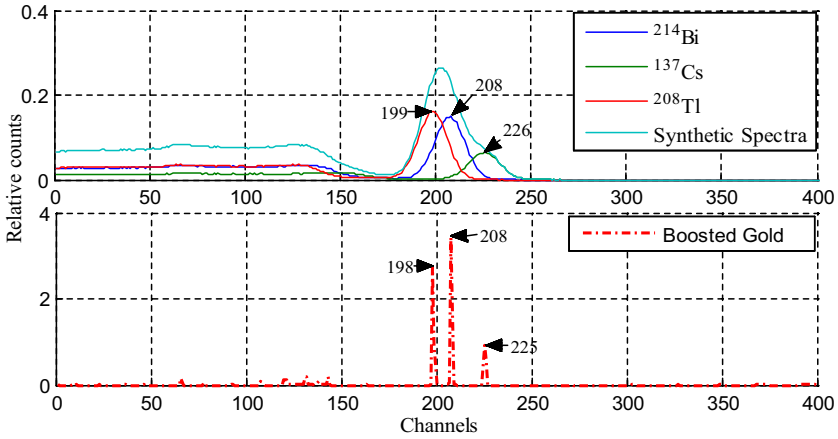

Fig. 5 Sample 2 results of Gaussian response matrix inversion decomposition

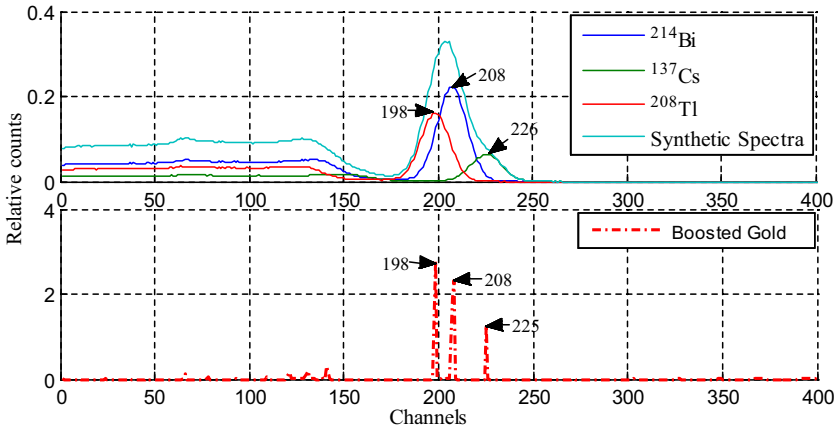

Fig. 6 Sample 3 results of Gaussian response matrix inversion decomposition

$E = 2.9577$ keV/channel, such that the peak position was located at channel 225.8 between channels 225 and 226, which resulted in a peak channel of 225 rather than 226 for Samples 2 and 3.

Regardless of deviations in the peak area ratios or peak positions owing to the deconvolution method, the results will be influenced by the FWHM calibration. Therefore, the accuracy of the FWHM calibration directly affects the analytical results. The test of the Gaussian response matrix for the decomposition of overlapping spectral peaks demonstrated that, for an NaI(Tl) detector with a resolution of about 8 %, representative of a FWHM of about 52 keV, the deviations of the peak positions of overlapping peaks were between 52.2 and 26 keV (that is, between 0.5 and 1 FWHM) in the samples with different proportions. As such, the Gaussian deconvolution response matrix accurately determined the peak positions and peak areas.

4.2 Test and analysis of U series and Th series experimental spectra

The experimental spectra of ^{238}U and ^{232}Th radionuclide series were tested to validate the feasibility of the proposed method in practical applications. The radioactive sources used in the experiment adopt the ^{238}U radionuclide series with mass fraction of 186×10^{-6} and specific activity of 2308.26 Bq/kg, and the ^{232}Th radionuclide series with the mass fraction of 157×10^{-6} and specific activity of 638.99 Bq/kg, and their physical conditions are solid and shapes are globular. Experimental spectra were obtained using a NaI(Tl) detector with an energy resolution of 7.9 % and dimensions 75 mm$\Phi \times 75$ mm, and a custom developed 1024 channel digital signal processor (DSP) multichannel spectrometer with a universal serial bus (USB) interface, integral nonlinearity <0.1 %, differential nonlinearity <0.2 % energy 50–3000 keV, counting rate >20 k, automatic spectra stabilization, and an energy calibration $E = 2.9577$ keV/ch. The relative measurement method was employed in all tests.

4.2.1 Analysis of the characteristic peaks of the ^{238}U radionuclide series

The ^{238}U series gamma-ray spectra are mainly comprised of the 0.242, 0.295, and 0.352 MeV characteristic peaks generated by ^{214}Pb and the 0.609, 0.787, 1.1203, and

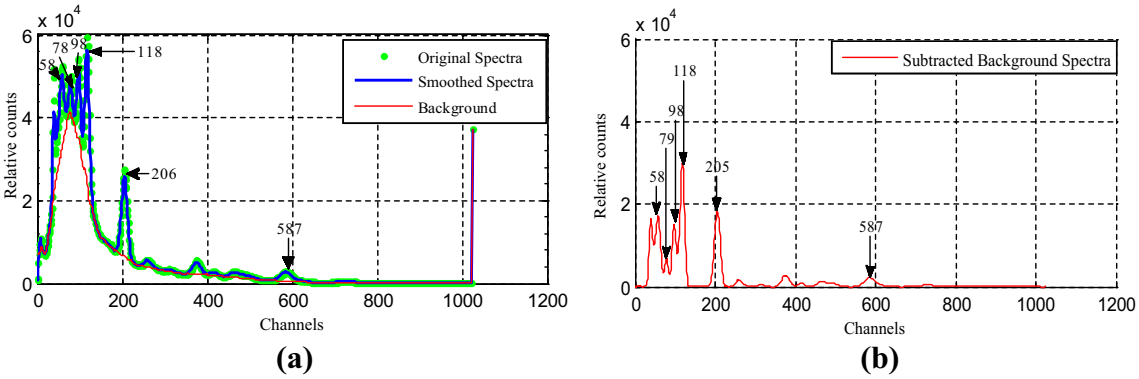

Fig. 7 The ^{238}U radionuclide series spectrum after background subtraction. **a** The ^{238}U radionuclide series spectrum and **b** the spectrum after background subtraction

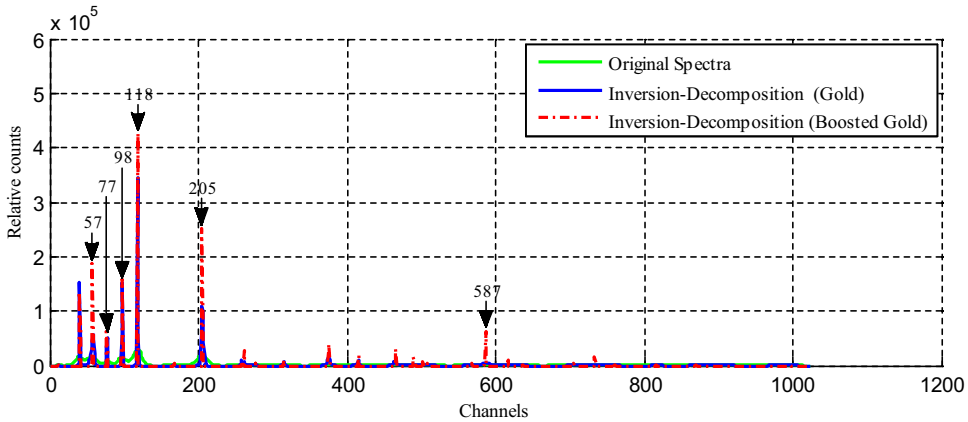

Fig. 8 Results of inversion decomposition for the ^{238}U radionuclide series

1.7645 MeV characteristic peaks generated by ^{214}Bi. To avoid the effect of low-energy peaks, the characteristic peaks of energies 0.609 and 1.7645 MeV were employed for the generally analysis. In the decomposition of overlapping peaks, the impact of the left side of the 0.511 MeV annihilation peak and the 0.583 MeV characteristic peak generated by ^{208}Tl of the ^{232}Th radionuclide series should be considered in the analysis of its characteristic peak. The ^{238}U radionuclide series employed in the adaptive FWHM process after background subtraction is shown in Fig. 7. The results of applying the Gaussian response matrix for decomposing the ^{238}U series experimental spectrum are shown in Fig. 8.

The characteristic peaks shown in Fig. 8 at channels 57, 77, 98, 118, 205, and 587, respectively, correspond to gamma energies of 0.176 MeV (0.1862 MeV characteristic peak generated by ^{226}Ra), 0.231 MeV (0.242 MeV characteristic peak generated by ^{214}Pb), 0.292 MeV (0.295 MeV characteristic peak generated by ^{214}Pb), 0.350 MeV (0.352 MeV characteristic peak generated by ^{214}Pb), 0.350 MeV (0.352 MeV characteristic peak generated by ^{214}Pb), and 1.74 MeV (1.764 MeV characteristic peak generated by ^{214}Bi). These results verify the practicability of the Gaussian response matrix method for decomposing the low-energy spectrum of the ^{238}U series.

4.2.2 *Analysis of the characteristic peaks of the ^{232}Th radionuclide series*

The ^{232}Th radionuclide series is mainly comprised of the 0.239 MeV characteristic peak generated by ^{212}Pb and the 0.511, 0.583, and 2.615 MeV characteristic peaks generated by ^{208}Tl. Because the 2.615 MeV characteristic peak generated by ^{232}Th was the highest energy peak with the strongest intensity, was subjected to no significant interference near its energy window, and was relatively weakly affected by the background, the 2.615 MeV characteristic peak was employed for the generally analysis. The ^{232}Th radionuclide series employed in the adaptive FWHM process after background subtraction is shown in Fig. 9. The results of applying the Gaussian response matrix for decomposing the ^{232}Th series experimental spectrum are shown in Fig. 10.

In Fig. 8 or 10 spectra obtained after applying the Gold and Boosted Gold decomposition to the measured spectra, very narrow photopeaks are observed with the counts concentrated to several channels. But the counts should be the same, because the photopeaks after the Gold and Boosted Gold decomposition are concentrated into several channels with practically no change of the area of the

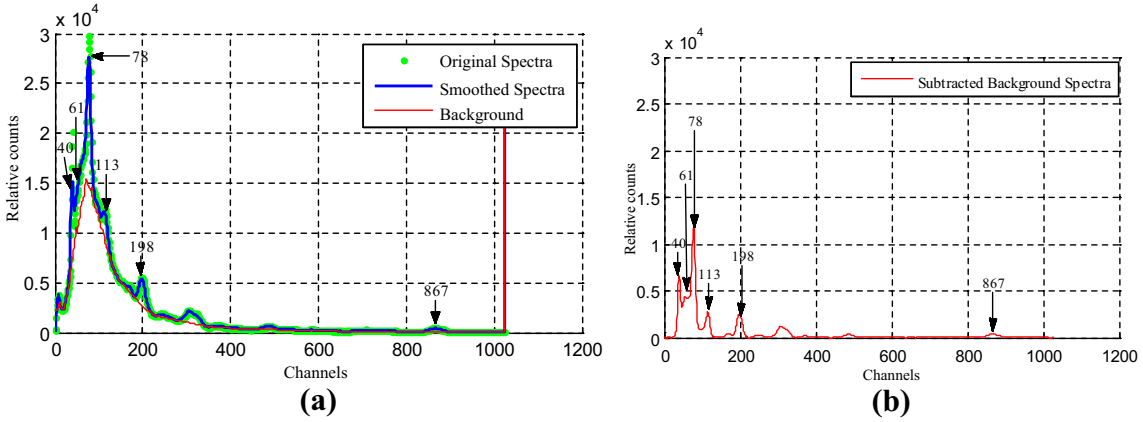

Fig. 9 The ^{232}Th radionuclide series spectrum after background subtraction. **a** The ^{232}Th radionuclide series spectrum and **b** the spectrum after background subtraction

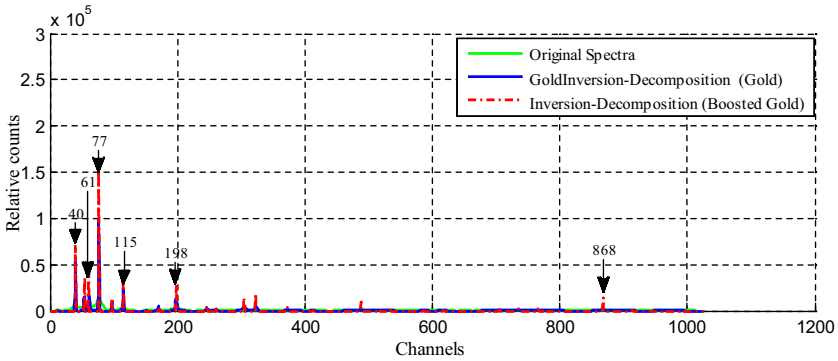

Fig. 10 Results of inversion decomposition for the ^{232}Th radionuclide series

photopeak comparing with the photopeaks obtained from the original spectra. In other words, the total count of decomposed spectra is roughly equal to the number of photons that came from undecomposed photon sources which were incident to the crystal detector. The characteristic peaks shown in Fig. 10 at channels 40, 77, 115, 198, and 868, respectively, correspond to 0.119 MeV (0.129 MeV characteristic peak generated by ^{228}Ac), 0.229 MeV (0.239 MeV characteristic peak generated by ^{214}Pb), 0.341 MeV (0.338 MeV characteristic peak generated by ^{228}Ac), 0.585 MeV (0.583 MeV characteristic peak generated by ^{208}Tl), and 2.578 MeV (2.615 MeV characteristic peak generated by ^{208}Tl). These results also verify the feasibility of the proposed spectrum analysis.

4.2.3 Analytical results of the U and Th series experimental spectra

Figures 8 and 10 show that analytical results of the low-energy components of the spectra are more complex and less reliable. The reasons for this can be given as follows: (1) The spectrum lines in the low-energy region are affected by the natural background and inverse scattering peaks, which leads to an incomplete subtraction of the background. (2) The FWHM values in the low-energy spectrum region are narrow, and the response matrix, being restricted to integer channels, results in correspondingly large amplitude variations in the FWHM values, which greatly affects the analytical accuracy. (3) The accuracy of the FWHM calibration in the low-energy range is reduced relative to that in the high-energy range. The Gaussian response characteristics of the deconvolution method are less sensitive to the interference of peak noise when the impulse response has a wider FWHM, such that it is better to select wider Gaussian peak widths in the low-energy range of the spectrum, which would provide for more accurate linear FWHM calibrations in the low-energy range of the spectrum.

5 Conclusion

An inversion decomposition method for gamma spectrum analysis based on a Gaussian response matrix was proposed. According to the physical characteristics of spectra formation and detector features, the photoelectric peaks representative of gamma photons with different energies in an NaI(T1) detector present unique FWHM values. The statistical properties of spectra also show that

the photoelectric peaks are approximately Gaussian in shape. Therefore, a response matrix comprised of Gaussian functions based on an adaptive FWHM process was proposed. Improved Gold and Boosted Gold algorithms were employed to accelerate the decomposition of the measured spectrum and to distribute a characteristic peak within a few narrow channels. Spectrum decomposition speed tests on a PC based on a total of 1024 channels resulted in the Gold algorithm requiring 4600 iterations, i.e., 8.8 s, while the Boosted Gold algorithm required about 6800 iterations, i.e., 1.1 s for an equivalent spectrum decomposition. The proposed inversion decomposition method was employed to analyze experimental spectra, including the ^{238}U and ^{232}Th radionuclide series, where the results verified the practicability of the Gaussian response matrix method, particularly in the low-energy region of the spectrum. Among the advantages of the proposed method, the use of the Gaussian response matrix for spectrum decomposition involves a relatively slight computational burden. Precise measurement of the FWHM values during calibration results in a more accurately decomposed spectrum. Furthermore, the method is applicable after background subtraction. As such, the inversion decomposition method using the Gaussian response matrix provides a useful method for the qualitative and quantitative analysis of gamma spectra. The new decomposition method is expected to contribute toward the development of intelligent nuclear analysis instruments, making gamma spectroscopy methods widely applicable to mineral exploration and radioactive monitoring.

References

1. B.D. Milbrath, B.J. Choate, J.E. Fast et al., Comparison of LaBr 3: Ce and NAI(Tl) scintillators for radio-isotope identification devices. Nucl. Instrum. Methods A **572**, 774–784 (2007). doi:10.1016/j.nima.2006.12.003
2. X.M. Fang, L.I. Xin-Nian, Comparison of performances of NaI and HPGe detectors. J. Shanghai Univ Nat. Sci. Ed. **10**, 389–392 (2004). doi:10.3969/j.issn.1007-2861.2004.04.013
3. A. Likar, T. Vidmar, A peak-search method based on spectrum convolution. J. Phys. D Appl. Phys. **36**, 1903–1909 (2003). doi:10.1088/0022-3727/36/15/323
4. M.H. Zhu, L.G. Liu, Q.I. Dong-Xu et al., Least square fitting of low resolution gamma ray spectra with cubic B-spline basis functions. Chin. Phys. C **33**, 24–30 (2009). doi:10.1088/1674-1137/33/1/006
5. M. Morhác, An algorithm for determination of peak regions and baseline elimination in spectroscopic data. Nucl. Instrum. Methods A **600**, 478–487 (2009). doi:10.1016/j.nima.2008.11.132
6. J.F. Pang, *Gamma Energy Spectrum Analysis* (Shanxi Science and Technology Press, Xi'an, 1993), pp. 350–716
7. J.F. He, Q.F. Wu, J.P. Cheng et al., An Inversion Decomposition Test Based on Monte Carlo Response Matrix on the Gamma Ray Spectra from NaI(Tl) Scintillation Detector, in *Journal of Nuclear Science and Technology*, ed. by L.H. Sun (Springer, Singapore, 2016)
8. B. Tang, L.Q. Ge, F. Fang et al., *The Principle of Measurement on Nuclear Radiation* (Harbin Engineering University Press, Harbin, 2010), pp. 161–215
9. Gordon R. Gilmore, *Practical Gamma-ray Spectrometry*, 2nd edn. (Nuclear Training Services Ltd, Warrington, 2008). doi:10.1002/9780470861981
10. R.P. Gardner, X. Ai, C.R. Peeples et al., Use of an iterative convolution approach for qualitative and quantitative peak analysis in low resolution gamma-ray spectra. Nucl. Instrum. Methods A **652**, 544–549 (2011). doi:10.1016/j.nima.2010.12.224
11. M.S. Rahman, G. Cho, Unfolding low-energy gamma-ray spectrum obtained with NaI(Tl) in air using matrix inversion method. J. Sci. Res. **2**, 221–226 (2010). doi:10.3329/jsr.v2i2.4372
12. M. Morhác, V. Matoušek, Complete positive deconvolution of spectrometric data. Digit. Signal Process. **19**, 372–392 (2009). doi:10.1016/j.dsp.2008.06.002
13. J.L. Zheng, Q.X. Ying, W.L. Yang, *Signals and Systems* (Higher Education Press, Beijing, 2011), pp. 28–130
14. M.S. Rahman, G. Cho, B.S. Kang, Deconvolution of gamma-ray spectra obtained with NaI(Tl) detector in a water tank. Radiat. Prot. Dosim. **135**, 203–210 (2009). doi:10.1093/rpd/ncp102
15. R.L. Heath, *Scintillation Spectrometry Gamma-Ray Spectrum Catalogue*, vol. 1(Rev), 2nd edn. (γ-Ray Spectrometry Center Idaho National Engineering and Environmental Laboratory, Idaho, 1997). doi:10.2172/4033555
16. Y. Wang, Y. Wei, Implicit FWHM calibration for gamma-ray spectra. J. Nucl. Sci. Technol. **24**(020403–297), 2013 (2013). doi:10.13538/j.1001-8042/nst.02.005
17. R. Gold, in *An Iterative Unfolding Method for Response Matrices*, vol. III. AEC Research and Development Report ANL-6984. Argonne National Laboratories, Argo. (1964). doi: 10.2172/4634295
18. S. Wachtmeister, S. Csillag, Implementation of gold deconvolution for enhanced energy resolution in EEL spectra. Ultramicroscopy **111**, 79–89 (2011). doi:10.1016/j.ultramic.2010.10.006
19. P. Bandzuch, M. Morhac, J. Kristiak, Study of the Van Cittert and Gold iterative methods of deconvolution and their application in the deconvolution of experimental spectra of positron annihilation. Nucl. Instrum. Methods A **384**, 506–515 (1997). doi:10.1016/S0168-9002(96)00874-1
20. M. Guttormsen, T.S. Tveter, L. Bergholt et al., The unfolding of continuum γ-ray spectra. Nucl. Instrum. Methods A **374**, 371–376 (1996). doi:10.1016/0168-9002(96)00197-0
21. M. Miroslav, J. Klimanb, V. Matousek et al., Background elimination methods for multidimensional coincidence γ-ray spectra. Nucl. Instrum. Methods A **401**, 113–132 (1997). doi:10.1016/S0168-9002(97)01023-1
22. C. Xu, I. Aissaoui, S. Jacquey, Algebraic analysis of the Van Cittert iterative method of deconvolution with a general relaxation factor. J. Opt. Soc. Am. A **11**, 2804–2808 (1994). doi:10.1364/JOSAA.11.002804
23. M. Jandel, M. Morhac, J. Kliman et al., Decomposition of continuum γ-ray spectra using synthesized response matrix. Nucl. Instrum. Methods A **516**, 172–183 (2004). doi:10.1016/j.nima.2003.07.047